PHOTONIC SENSORS / Vol. 10, No. 1, 2020: 67–79

Graphene-Coated Optical Fiber SPR Biosensor for BRCA1 and BRCA2 Breast Cancer Biomarker Detection: a Numerical Design-Based Analysis

Md. Biplob HOSSAIN[1*], Md. Muztahidul ISLAM[2], Lway Faisal ABDULRAZAK[3], Md. Masud RANA[4], Tarik Bin Abdul AKIB[2], and Mehedi HASSAN[2]

[1]*Dept. of Electrical and Electronic Engineering, Jashore University of Science and Technology, Jashore-7408, Bangladesh*

[2]*Dept. of Electrical and Electronic Engineering, Bangladesh Army University of Engineering and Technology, Natore-6431, Bangladesh*

[3]*Dept. of Computer Science, Cihan University Slemani, Sulaimaniya-46001, Iraq*

[4]*Dept. of Electrical and Electronic Engineering, Rajshahi University of Engineering & Technology, Rajshahi-6402, Bangladesh*

[*]Corresponding author: Md. Biplob HOSSAIN E-mail: biplobh.eee10@gmail.com

Abstract: This paper provides a simple hybrid design and numerical analysis of the graphene-coated fiber-optic surface plasmon resonance (SPR) biosensor for breast cancer gene-1 early onset (BRCA1) and breast cancer gene-2 early onset (BRCA2) genetic breast cancer detection. Two specific mutations named 916delTT and 6174delT in the BRCA1 and BRCA2 are selected for numerical detection of breast cancer. This sensor is based on the technique of the attenuated total reflection (ATR) method to detect deoxyribonucleic acid (DNA) hybridization along with individual point mutations in BRCA1 and BRCA2 genes. We have numerically shown that momentous changes present in the SPR angle (minimum: 135% more) and surface resonance frequency (SRF) (minimum: 136% more) for probe DNA with various concentrations of target DNA corresponding to a mutation of the BRCA1 and BRCA2 genes. The variation of the SPR angle and SRF for mismatched DNA strands is quite negligible, whereas that for complementary DNA strands is considerable, which is essential for proper detection of genetic biomarkers (916delTT and 6174delT) for early breast cancer. At last, the effect of electric field distribution in inserting graphene layer is analyzed incorporating the finite difference time domain (FDTD) technique by using Lumerical FDTD solution commercial software. To the best of our knowledge, this is the first demonstration of such a highly efficient biosensor for detecting BRCA1 and BRCA2 breast cancer. Therefore, the proposed biosensor opens a new window toward the detection of breast cancers.

Keywords: ATR; BRCA1; BRCA2; cancer; DNA hybridization; graphene, SPR; SRF; 6174delT; 916delTT

Citation: Md. Biplob HOSSAIN, Md. Muztahidul ISLAM, Lway Faisal ABDULRAZAK, Md. Masud RANA, Tarik Bin Abdul AKIB, and Mehedi HASSAN, "Graphene-Coated Optical Fiber SPR Biosensor for BRCA1 and BRCA2 Breast Cancer Biomarker Detection: a Numerical Design-Based Analysis," *Photonic Sensors*, 2020, 10(1): 67–79.

1. Introduction

A great deal of attention on surface plasmon resonance (SPR) with graphene based biosensors as a leading optical sensing technology has been

Received: 5 January 2019 / Revised: 25 March 2019

DOI: 10.1007/s13320-019-0556-7
Article type: Regular

achieved by the researchers because of their effective applications in numerous fields including medical diagnostics, biomolecule detection, biochemical detection and environmental monitoring [1–3], and proteins and deoxyribonucleic acid (DNA) hybridization [4, 5]. DNA hybridization is a regularly used biomolecular method by which the level of the genetic relationship between pools of DNA sequences to obtain the genetic gap of two organisms has been estimated. This biochemical process of identifying DNA nucleotide bonding in the proper orientation is very important for medical diagnostics [6] even for BRCA1 and BRCA2 genes in early breast cancer diagnosis [2–4]. BRCA1: a gene that normally acts to restrain the growth of cells in the breast but which, when mutated, predisposes breast cancer. The BRCA1 gene belongs to a class of genes known as tumor suppressor genes. Like other tumor suppressor genes, BRCA1 regulates the cycle of cell division by keeping cells from growing and dividing too rapidly or in an uncontrolled way. In particular, it inhibits the growth of cells that line the milk ducts in the breast. BRCA2 is a gene that normally acts to restrain the growth of cells in the breast and ovary but which, when mutated, may predispose breast cancer and ovarian cancer. BRCA2 mutations have also been discovered to be responsible for a significant fraction of early-onset prostate cancer. The first breast cancer genes identified were BRCA1 and BRCA2. Mutations of BRCA1 and BRCA2 account for about half of all cases of inherited breast cancer. These tumors tend to occur in young women. BRCA1 and BRCA2 are usually not involved in breast cancer that is not hereditary. The genetic tendency is responsible for 5% – 10% breast cancer, and over 75% – 80% of inherited breast cancer cases are owing to mutations in BRCA1 and BRCA2 genes [1, 2].

These genes are tumor suppressor genes associated with double strand deoxyribonucleic acid (dsDNA) repair accounting for abnormal uncontrolled tumor cell growth [2]. More than 400 different mutations in BRCA1 and BRCA2 genes are leading to tumor growth and thus finally cancer [3]. Real-time detection of polymerase chain reaction (PCR) technologies has become the most merchandized detection approach with high specificity and sensibility [3]. Two prime categories, genetic and proteomic, are classified for breast cancer biomarkers. Moreover, BRCA1, BRCA2, and phosphoprotein tumor suppressor (p53) are genetic. And adipose tissue macrophages gene (ATM), cancer antigen gene 125 (CA125), cancer antigen gene 153 (CA153), carcinoembryonic antigen (CEA), checkpoint kinase 2 (CHEK2), human epidermal growth factor receptor 2 (HER2), phosphatase and tensin homolog (PTEN), and serine/threonine kinase 11 (STK11) are proteomic markers, which are also liable for breast cancer risk [4, 5]. Every year, above 350 000 deaths and 192 000 new cases are reported due to breast cancer [4]. At present, ultrasound, mammography, PCR screening, and other approaches have been applied to identify the diagnosis of breast cancer. But this tumor is difficult to identify, because of its tiny in size [4, 6]. Thus, effective and precise approaches to breast cancer recognition and monitoring are urgently required. To meet the requirement of effective and precise approaches to breast cancer recognition, the SPR technology is being used to obtain the information on DNA molecular bonding, by which BRCA1 and BRCA2 breast cancers are directly diagnosable [2–5].

Fundamentally, SPR is a charge density oscillation at the metal-dielectric interface stimulated by transverse mode (TM) polarized electromagnetic waves, typically known as surface plasmon wave (SPW) [7]. The SPW at the interface between a metal (e.g., Au, Ag, or Al) and a dielectric is used by the SPR biosensor to investigate the interactions between biomolecules [8, 9]. And these interactions are accomplished by the practice of an

optical fiber-based SPR sensor. A fiber optic SPR sensor has lots of advantages such as the lightness in weight, compactness, high sensitivity, ease of multiplexing and remote sensing, mechanical flexibility, and ability to transmit optical signals over a long distance, which allows miniaturization and chemical or biological sensing in inaccessible locations [9]. As a fundamental part of the fiber optic SPR biosensor, a fiber is coated with a thin metallic film (Au, Ag, or Al), for example Au, in our study for the distinction of the sensing medium and the dielectric [8]. Here, the sensing layer is used to functionalize the gold film, which consequently improves the absorption of biomolecules [8]. An essential constituent of the SPR sensing device is a large surface area-based absorbing material; recently, developed two-dimensional (2D) nanomaterial graphene has satisfied this requirement [10].

The sensitivity of the SPR sensor increases greatly when graphene is used as a sensing layer [11]. Graphene is a 2D material of graphite of one atom in thickness arranged in a honeycomb lattice. It shows many properties, such as high optical transparency, low reluctance, high carrier mobility, and tunability [12, 13]. In literature [14], graphene was used to improve sensor performance (sensitivity) as biomolecular recognition elements (BRE). For the excitement and propagation of surface plasmons, graphene can be used that has been proved experimentally and theoretically [9].

In this paper, a numerical modeling of graphene-coated fiber optic SPR biosensor for specific mutations named 916delTT and 6174delT in the BRCA1 and BRCA2, in which genetic early breast cancer is reported. Since graphene has prominent characteristics [15–18], a graphene monolayer is sandwiched between the gold film and sensing dielectric as an effective light absorption medium. We use θ_{SPR}-R_{min} (SPR angle-minimum reflectance), as detecting attributor, which enhances the sensitivity of 1+0.35×£ (where £ is the total of graphene coatings) and also use RFC-T_{max} (resonance frequency characteristics-maximum transmittance) attributor, which enhances the sensitivity of 1+0.36×£ compared with the conventional SPR sensor in [19–22]. This sensor is put in to recognize perfectly matched hybridization event (between shDNA and mrDNA sequence of BRCA1 gene (named 916delTT) and BRCA2 gene (named 6174delT), respectively as shown in Figs. 2(a) and 3(a) and mismatched hybridization event (between shDNA and wtDNA sequence of BRCA1 gene (916delTT) and BRCA2 gene (6174delT), respectively as shown in Figs. 2(b) and 3(b). Significant changes have been presented in the SPR angle and surface resonance frequency (SRF) curves for each of the mutations compared with those of the complementary target mutated type (mrDNA) sequences. Phosphate buffer saline (PBS) solution as bare sensing dielectric medium provides better adsorption of single strand DNA (mrDNA for perfectly matched hybridization and wtDNA for mismatched hybridization) biomolecules [23, 24]. The refractive indices (RI) of the graphene and gold (Au) nearby change owing to the immobilization of the 916delTT and 6174delT DNA molecule. The RI change will cause a change in the propagation constant of the SPR wave, which can be optically ascertained by the attenuated total reflection (ATR) method [7]. At the end of the present study, the effect of electric field distribution on inserting graphene layer is analyzed incorporating the finite difference time domain (FDTD) technique by using Lumerical FDTD solution commercial software.

2. Design methodology

2.1 Structural modeling of the bproposed sensor

The design structure of the proposed graphene-based fiber optic SPR biosensor is given in Fig. 1. Fiber optic SPR sensor has a core diameter of 50 μm and a cladding diameter of 50.25 μm [25].

In the sensor region, a 5-mm cladding is detached, and this slice of the cladding is considered to be implicated with a prism, gold (Au) thin film, and graphene with the thicknesses of d_p=74.5 nm, d_{Au}= 50 nm, and d_g=0.34 nm× £, respectively [7, 25]. This biosensor sensing region is involved with a total of four layers [22]. The first layer is a prism with high RI of n_p = 1.723 [25]. The second layer is Au, deposited on the base of the prism with complex RI of n_{Au}=0.1726 + 3.4218i [25]. The third layer is a graphene with high complex RI of n_g = 3 + 1.149106i. The fourth layer is a PBS solution as sensing dielectric medium [7, 22]. The graphene-based biosensor as a sensing dielectric adsorbs the complementary molecule by the receptor and produces a native increase in the RI at the graphene surface [22]. Once the moleculars interact, the immobilization surface can be renewed by applying an appropriate chemical with the intention of eliminating target DNA samples except denaturing the probe DNA [26, 27].

2.2 Mathematical modeling of the proposed sensor

In Fig. 1, the light acceptance cone is the angle of an incident light hitting the fiber core and totally reflected by the cladding. In our proposed fiber optic SPR sensor, TM polarized He-Ne (wavelength, λ = 633 nm) light is used as an incident light [7, 22]. The numerical results suggest that 633 nm He-Ne light allows the increased overall sensitivity of the sensor with the minimal possible Kerr effect [28].

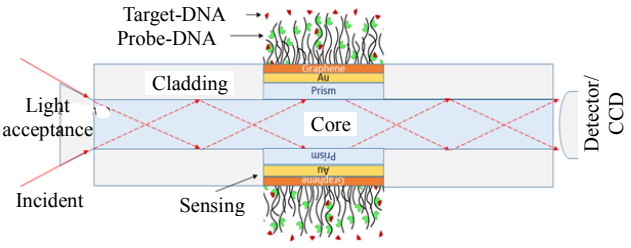

Fig. 1 Structural presentation of 4-layered model for the fiber optic SPR biosensor: prism, Au (50 nm), graphene (0.34£ nm), and PBS buffer solution which contains probe-DNA (p-DNA:shDNA) and complementary target mutated type (tDNA:mrDNA) or wild-type (tDNA:wtDNA) samples.

The light is launched into one end, and the power available of the other end (dP_T) with the incident angle θ can be expressed as [25, 29]

$$\mathrm{d}P_T \propto \left[\frac{n_c^2 \sin\theta\cos\theta}{(1-n_c^2\cos^2\theta)^2}\right]\mathrm{d}\theta \tag{1}$$

where n_c (1.451) is the refractive index of the fiber core. The normalized transmitted power of p-polarized TM light is expressed at the core-prism-metal try interface as [25, 29]

$$P_T = \frac{\int_{\theta_{cr}}^{\Pi/2} R_P^{\left(\frac{L}{D\tan\theta}\right)}\left[\frac{n_c^2\sin\theta\cos\theta}{(1-n_c^2\cos^2\theta)^2}\right]\mathrm{d}\theta}{\int_{\theta_{cr}}^{\Pi/2}\left[\frac{n_c^2\sin\theta\cos\theta}{(1-n_c^2\cos^2\theta)^2}\right]\mathrm{d}\theta} \tag{2}$$

where L (5 mm) is the length of the sensing region, D (50 μm) is the diameter of the fiber core, and θ_{cr} is the critical angle of the optical fiber [expressed as $\theta_{cr}=a\sin(n_{cl}/n_c)$], where n_{cl} is the refractive index of the fiber cladding. The reflected power R can be obtained by four-layered (prism, metal, graphene, and sensing layers) Fresnel's model analysis as [25]

$$R=|r_p|^2 \tag{3}$$

where

$$r_p = \frac{(F_{11}+F_{12}n_N)n_1-(F_{21}+F_{22}n_N)}{(F_{11}+F_{12}n_N)n_1+(F_{21}+F_{22}n_N)}. \tag{4}$$

In (4), F is defined in [25] as

$$F_{ij} = \left[\prod_{k=2}^{3}\begin{pmatrix}\cos\beta_k & -\dfrac{\mathrm{i}\sin\beta_k}{n_k}\\ -\mathrm{i}n_k\sin\beta_k & \cos\beta_k\end{pmatrix}\right]_{ij} = \begin{bmatrix}F_{11} & F_{12}\\ F_{21} & F_{22}\end{bmatrix} \tag{5}$$

where n_k is the arbitrary transverse refractive indices of the corresponding kth layer which can be explained by [25, 29]

$$n_k = \left[\frac{\mu_k}{\varepsilon_k}\right]^{1/2}\cos\theta_k = \sqrt{\frac{\varepsilon_k-(n_p\sin\theta_{in})^2}{\varepsilon_k^2}} \tag{6}$$

and β_k is the arbitrary phase constant of the corresponding kth layer which can be explained by [22, 25]

$$\beta_k = \frac{2\pi}{\lambda}n_k\cos\theta_k(z_k-z_{k-1}) = \frac{2\pi}{\lambda}d_k\sqrt{\varepsilon_k-(n_p\sin\theta_{in})^2} \tag{7}$$

where z_k is the wave impedance of the kth layer and is defined as [48]

$$z_k = \frac{k_{\text{light}} n_k \cos\theta_k}{(2\pi c / \lambda_{633})\varepsilon_k^{\,2}} \tag{8}$$

and θ_k is the incident angle of the kth layer and is defined as [22]

$$\theta_k = a\cos\left(\sqrt{1-(n_{k-1}/n_k)\sin^2\theta_{\text{in}}}\right). \tag{9}$$

In (5) to (9), n_p is the RI of the prism, θ_{in} is the initial incident angle indicated in (13), ϵ_k is the permittivity of the kth layer dielectric, and d_k is the thickness of the kth layer (thickness of mono layer graphene d_g= 0.34 nm, thickness of gold d_{Au}=50 nm), respectively. For TM polarization, the electric field generated owing to the SPW along the x direction is specified in [30] as

$$E_x = E_0 \cos\theta_{\text{in}} \mathrm{e}^{\left(-\mathrm{i}k_{\text{spw}}\cos\theta_{\text{in}} z - \mathrm{i}k_{\text{spw}}\sin\theta_{\text{in}} x\right)} \tag{10}$$

where $k_{\text{spw}} = k_0 n_k$ is the wave vector of SPW in the layered media described by (11), $k_0 = 2\pi c_0 / \sqrt{(\mu_0\varepsilon_0)\lambda_{633}}$ is a free-space wave vector, and E_0 is the magnitude of the electric field. The SPW propagates along the horizontal direction with the propagation constant k_{spw}, described in (11), where n_{Au} is the RI of the gold, and n_s is the RI of the sample [22]:

$$k_{\text{SPW}} = \frac{2\pi}{\lambda_{633}}\sqrt{\frac{n_{\text{Au}}^2 n_S^2}{n_{\text{Au}}^2 + n_S^2}}. \tag{11}$$

The SPW propagates in a different propagation constant, which is known as surface plasmon resonance point (SPRP) [7, 22, 31]. The frequency at the SPRP is called SRF. If SPW changes, it makes the SRF change which is given by [22]

$$SRF = \frac{k_{\text{SPW}} c}{2\pi\sqrt[3]{n_{\text{Au}} n_S n_G}} \tag{12}$$

where c is the light speed. Transmittance vs. *SRF* curve is normally known as surface plasmon resonance frequency (SPRF) response. A four-layered Fresnel model is applied to create an SPRF curve, for the proposed fiber optic SPR sensor to determine the transmitted light intensity. The reflectance vs angle of incidence or reflectance vs wavelength characteristics curve is known as the SPR curve. The SPR angle can be represented as [7, 22]

$$\theta_{\text{SPR}} = a\sin\left[\frac{1}{n_P}\sqrt{\frac{n_{\text{Au}}^2 n_s^2}{(n_{\text{Au}}^2 + n_s^2)}}\right]. \tag{13}$$

The shifting characteristics of the SPR angle owing to the variation of the RI are established as the following form [18–25]:

$$\begin{aligned}\delta n_s &= n_s^{\text{final}} - n_s^{\text{init}} \\ &= n_s^{\text{init}} + c_a \frac{\mathrm{d}n}{\mathrm{d}c} - n_s^{\text{init}} \\ &= c_a \frac{\mathrm{d}n}{\mathrm{d}c}.\end{aligned} \tag{14}$$

Equation (14) shows how the refractive index is changed after the hybridization with different concentrated complementary targets DNA (tDNA: wtDNA) or mismatched targets DNA (tDNA: mrDNA) of BRCA1 and BRCA2 genes with PBS solutions. The SPR angle and SRF are refractive index dependent parameters of the sensing medium. Here, n_s^{init} (= sensing medium initial refractive index) is the refractive index (RI) of the sensing dielectric before adsorption of shDNA (pDNA) molecule. When the dielectric sample (probe or target) is absent inside the sensing medium, n_s^{init} is the RI of PBS saline (n_4 = 1.34 RIU), which is available in the bare sensor. c_a is the concentration of adsorbed bio molecules, for example, if 1000 nM concentrated mrDNA has been added into the sensing medium, the value of c_a is 1000 nM. dn/dc is the RI growth factor, supposing that after adding 1000 nM concentrated molecules, the RI of the sensing layer has been changed because the sensing layer now consists of not only PBS but also 1000 nM concentrated molecules. The changed value of RI from PBS is dn/dc (= 0.181 cm^3/gm for PBS as the bare case [16]). And n_s^{final} is the RI of the sensing dielectric after adsorption of mrDNA. PBS is made of 0.0003 mol of NaH_2PO_4 (monosodium phosphate), 0.0016 mol of Na_2HPO_4 (disodium phosphate), 0.022 mol of NaCl, and 0.00054 mol of KCl mixed in milli-Q water [24]. PBS buffer solution allows easy discrimination of perfectly matched DNA from mismatched DNA

sequences [24]. The RI increment parameter is a (dn/dc) value of $0.18\pm0.03\,cm^3/g$, irrespective of the identity of the protein and the buffer ions in the occasion of utilizing PBS buffer solution [19]. The sensitivity of the optical SPR sensor is defined as the ratio of the change of output parameters (SRF or θ_{SPR}) to the change in the concentration of biomolecules, Δc_a [7, 22].

2.3 Designated DNA sequences for detection of breast cancer

In this study, we have selected 916delTT and 6174delT (two specific mutations) from the BRCA1 and BRCA2 genes for the detection of breast cancer. Mutated type (mrDNA) oligonucleotide signifies that the total complementary sequence and wild-type (wtDNA) oligonucleotide represent the total mismatched sequence to the immobilized mutated one [27]. Immobilization mutant (shDNA) oligonucleotide, control target (mfDNA) oligonucleotide, and mrDNA and wtDNA oligonucleotide sequence orientation specifications data of 916delTT and 6174delT are tabulated in Tables 1 and 2 [2, 27, 32]. Probe DNA (pDNA) sequence (shDNA), target fully complementary sequence (mrDNA), and target mismatched sequence (wtDNA) are shown in blue, green, and red colors, respectively, whereas control target sequence (mfDNA) is shown in the black color.

Perfectly matched hybridization event between shDNA sequence and mrDNA sequence in 916delTT and 6174delT specific mutations in BRCA1 and BRCA2 genes reveals the biomarker of genetic breast cancer, shown in Figs. 2(a) and 3(a), respectively. On the other hand, Figs. 2(b) and 3(b) are the figural representations of mismatched hybridization event between the wtDNA sequence and mrDNA sequence in 916delTT and 6174delT specific mutations in BRCA1 and BRCA2 genes, which revealed the biomarker of no possibility of genetic breast cancer.

The perfectly matched hybridization between the shDNA sequence and mrDNA sequence or mismatched hybridization between the shDNA sequence and wtDNA sequence of samples 916delTT and 6174delT is numerically performed in concentrations ranging from 1 nM to100 nM in the PBS solution. The mfDNA oligonucleotide, HCL, and the appropriate chemical have flowed in the PBS solution with the intention of eliminating target DNA samples and regeneration of pDNA [27].

Table 1 Sequence orientation of adenine (A), thymine (T), guanine (G), and cytosine (C) sequence in BRCA1 (916delTT).

Immobilized mutant (shDNA) sequence	5´-SH-$(CH_2)_6$-TTT TTT TTT TTT TTT GTT CTG TCA AACT – 3´
Mutated type (mrDNA) target sequence	5´-TGC CAC ATG GCT CCA CAT GCA AGT TTG ACA GAA CTA CCC TGA TAC TTT TCT GGA TGCC – 3´
Wild type (wtDNA) target sequence	5´-TGC CAC ATG GCT CCA CAT GCA AGT TTG AAA CAG AAC TAC CCT GAT ACT TTT CTG GAT GCC – 3´
Control target (mfDNA) sequence	5´-GGC ATC CAG AAA AGT ATC AGG GTA GTT CTG TTT CAA ACT TGC ATG TGG AGC CAT GTG GCA – 3´

Table 2 Sequence orientation of adenine (A), thymine (T), guanine (G), and cytosine (C) sequence in BRCA2 (6174delT).

Immobilized mutant (shDNA) sequence	5´- AGC TGG TCT GAC GTT TAT GAA TGT TCG TTACT – 3´
Mutated type (mrDNA) target sequence	5´-GGTA CGA CAC GAT TTT TAG GGAC TTC ATA AAC GTC TAC TCT GAC – 3´
Wild type (wtDNA) target sequence:	5´-GGTA CGA CAC GAT TTT TAG GGAC TTC ATC GAC ATC TAC TCT GAC– 3´
Control target (mfDNA) sequence:	5´- GTC AGA GTA GAT GTC GAT GAA GTC CCT AAA AAT CGT GTC GTACC – 3´

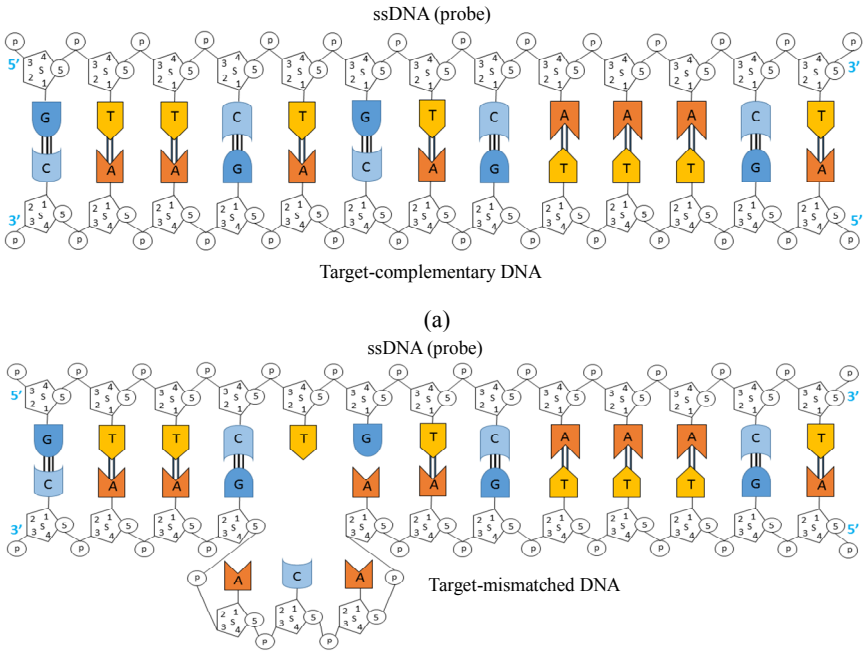

Fig. 2 Schematic of sequence orientation of adenine (A), thymine (T), guanine (G), and cytosine (C): (a) perfectly matched hybridization between shDNA and mrDNA sequences of BRCA1 gene (916delTT) and (b) mismatched hybridization between shDNA and wtDNA sequences of BRCA-1 gene (916delTT). Here, A-T bond by di-hydrogen bonding, G-C bond by tri-hydrogen bonding.

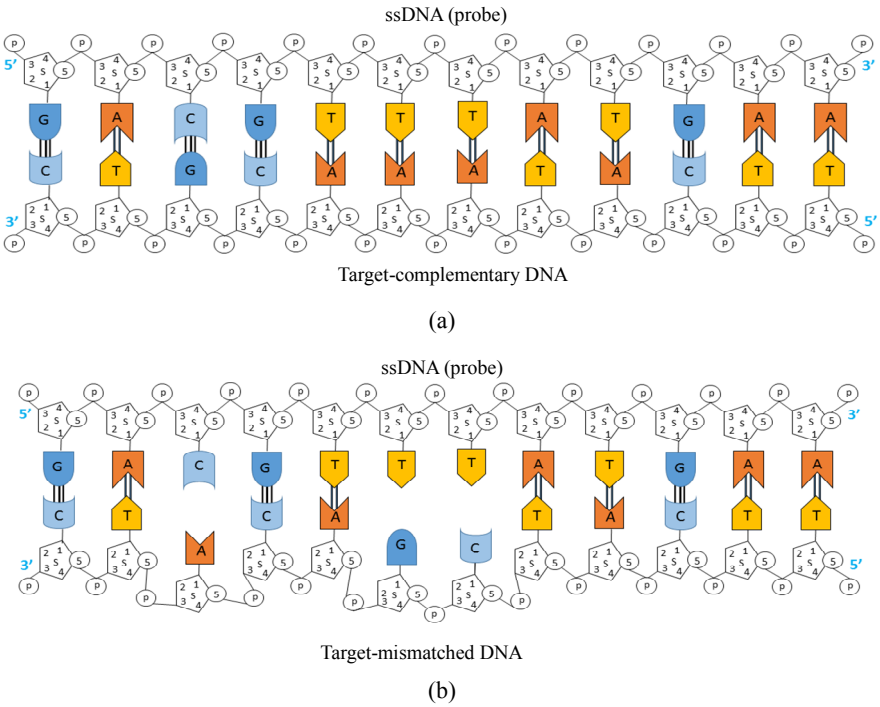

Fig. 3 Schematic of sequence orientation of adenine (A), thymine (T), guanine (G), and cytosine (C): (a) perfectly matched hybridization between shDNA and mrDNA sequences of BRCA2 gene (6174delT) and (b) mismatched hybridization between shDNA and wtDNA sequences. Here, A-T bond by di-hydrogen bonding, G-C bond by tri-hydrogen bonding.

3. Numerical results

Initially, a numerical study is presented to show the change of the SPR curve ($R_{\min}$ vs θ_{SPR}) and SPRF curve ($T_{\max}$ vs SRF) characteristics for the implication of the graphene layer and without implication of the graphene layer on the Au thin film.

Here, we use the PBS solution before adsorbing any DNA molecules. The θ_{SPR} and SRF without the graphene layer are 57.35° and 91.92 THz, and furthermore those with a single layer of graphene are 57.70° and 92.28 THz, respectively shown in Figs. 4(a) and 4(b). The SPR angle ($\delta\theta_{SPR}$= 0.35 °) and *SRF* (δSRF = 0.36 THz) have been increased due to adding the graphene film which is caused for enhancing the sensitivity of this sensor [11–14]. The detecting attributor's $\delta\theta_{SPR}$ and δSRF are shifting rightwards because of adding the graphene layer, as given in Table 3, as well as table data depicted in Figs. 4(a) and 4(b), respectively.

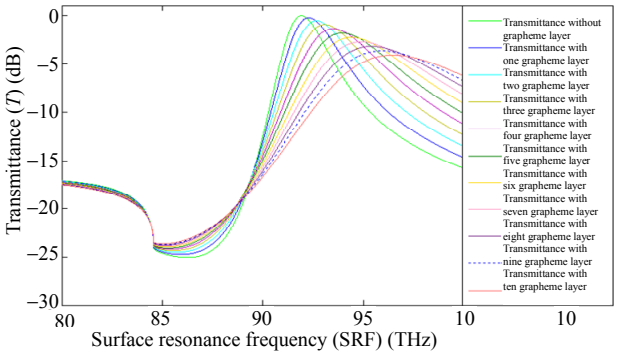

(a)

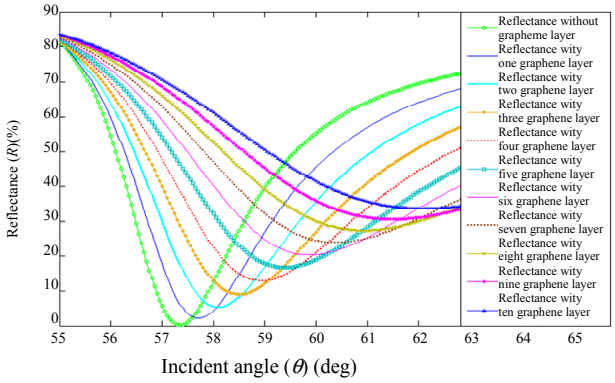

(b)

Fig. 4 Change in characteristics curves for (a) SPR curves and (b) SPRF curves for the fiber optic SPR biosensor without graphene and with graphene implicated sensor (for £ = 1, 2, 3,⋯, 10) before the adsorption of target BRCA DNA molecules.

Table 3 Data of R_{min}, θ_{SPR}, T_{max}, and *SRF* without graphene layer and with the total number of increasing graphene layer in fiber optic SPR biosensor.

Graphene layer	R_{min} (%)	θ_{SPR} (deg)	T_{max} (dB)	*SRF* (THz)	δR_{min} (%)	$\delta\theta_{SPR}$ (deg)	δT_{max} (dB)	δSRF (THz)
without layer (£ = 0nm)	0.25	57.35	0.0252	91.92	0.00	0.00	0.0000	0.00
1st layer (£ = 1 * 0.34nm)	2.26	57.70	0.2285	92.28	2.01	0.35	0.2033	0.36
2nd layer (£ = 2 * 0.34nm)	5.40	58.10	0.5550	92.68	5.15	0.75	0.5298	0.76
3rd layer (£ = 3 * 0.34nm)	9.05	58.50	0.9481	93.08	8.80	1.15	0.9229	1.16
6th layer (£ = 6 * 0.34nm)	20.38	59.85	2.2788	94.42	20.13	2.50	2.2536	2.50
8th layer (£ = 8 * 0.34nm)	27.31	60.90	3.1897	95.41	27.06	3.55	3.1645	3.49
9th layer (£ = 9 * 0.34nm)	30.51	61.50	3.6405	95.93	30.26	4.15	3.6153	4.01
10th layer (£=10 *0.34nm)	33.55	62.10	4.0867	96.47	33.30	4.75	4.0615	4.55

In Table 3, the breast cancer recognizing attributors R_{min}, θ_{SPR}, T_{max}, and *SRF* are almost proportionally increasing with an increase in the number of the graphene layer (£ = n * 0.34 nm; $1 \leq n \leq 10$) on the Au thin film. According to the calculation of the definition of sensitivity (S) in [7], if we use θ_{SPR}-R_{min} attributors, the sensitivity enhances to 135 % or more, and if we use *SRF*-T_{max} attributors, the sensitivity enhances 136 % or more based on the graphene monolayer implicated sensor, respectively compared with other operable SPR sensors in [7, 22].

Due to the addition of shDNA sequence (pDNA) on the sensing medium, RI increases because of increasing the concentration of the sensing medium followed by (14), and finally the θ_{SPR} and SPRF curves shift as depicted in Fig 5. The sensing parameters R_{min}, θ_{SPR}, *SRF*, and T_{max} are changing with different concentrated complementary mrDNAs and wtDNAs (ranging from 1 nm to 100 nm), which

are illustrated in the Figs. 5(a) and 5(b). Furthermore, table data have been extracted in Table 4. It is evidently decided that the significant right shift of θ_{SPR} and SPRF curve is a sign of perfectly matched hybridization happening in 916delTT and 6174delT with pDNAs [7, 22].

Figures 5(a) and 5(b) realistically explain the changes of R_{min} vs θ_{SPR} (SPR curve) characteristics and T_{max} vs SRF (SPRF curve) characteristics, respectively, without pDNA, with pDNA, and with flowing the specific concentrated complementary target wtDNA or wtDNAs of BRCA1 and BRCA2 genes. RI changes due to the immobilization of different concentrated breast cancer biomarker (916delTT and 6174delT) DNA molecules. The change of RI of the sensing medium has a significant impression on the SPRF and SPR curves. The significant right shift of θ_{SPR} and SRF is a sign of recognition of specific mutations 916delTT and 6174delT interaction with pDNAs, which also clarifies the detection of hereditary breast cancer.

The detecting parameter changes significantly with different concentrated mrDNAs, and these changes have been tabulated in Table 4, and accordingly, the decision will be made based on the detecting parameter.

In Table 4, the breast cancer recognizing attributors (δR_{min}, $\delta\theta_{SPR}$, δT_{max}, and δSRF) are calculated by choosing R_{min}, θ_{SPR}, T_{max}, and SRF values before adding pDNA as the standard.

After adding pDNA (shDNA), the interaction between pDNA to mismatched (wtDNA) DNA and pDNA to different concentrated perfectly matched target (mrDNA) DNAs has been calculated and tabulated in Table 4, in order to make a decision as accordingly in Table 5.

Table 4. Data of change of detecting attributors (δR_{min}, $\delta\theta_{SPR}$, δT_{max}, and δSRF) for introducing different concentrated target wtDNAs or mrDNAs of BRCA1 and BRCA2 genes.

Concentration (c_a) (nM)	R_{min} (%)	θ_{SPR} (deg)	T_{max} (dB)	SRF (THz)	$\delta R_{min}^{P-T} = \lvert R_{min}^{probe} - R_{min}^{target} \rvert$	$\delta\theta_{SPR}^{P-T}$ (deg) $= \lvert \theta_{SPR}^{probe} - \theta_{SPR}^{target} \rvert$	δT_{max}^{P-T} (dB) $= \lvert T_{max}^{probe} - T_{max}^{target} \rvert$	δSRF^{P-T} (THz) $= \lvert SRF^{probe} - SRF^{target} \rvert$
0 (no-probe)	2.26	57.75	0.2288	92.34	0.05	0.55	0.0051	1.04
1500 (shDNA)	2.31	58.30	0.2339	93.38	0.00	0.00	0.0000	0.00
1000 (wtDNA)	2.34	58.60	0.2368	93.94	0.03	0.30	0.0029	0.56
1500 (mrDNA)	2.40	59.10	0.2422	94.90	0.09	0.80	0.0083	1.52
1525 (mrDNA)	2.40	59.15	0.2427	94.99	0.09	0.85	0.0088	1.61
1550 (mrDNA)	2.41	59.20	0.2433	95.10	0.10	0.90	0.0094	1.72
1575 (mrDNA)	2.42	59.30	0.2441	95.22	0.11	1.00	0.0102	1.84
1600 (mrDNA)	2.42	59.35	0.2449	95.36	0.11	1.05	0.0110	1.98

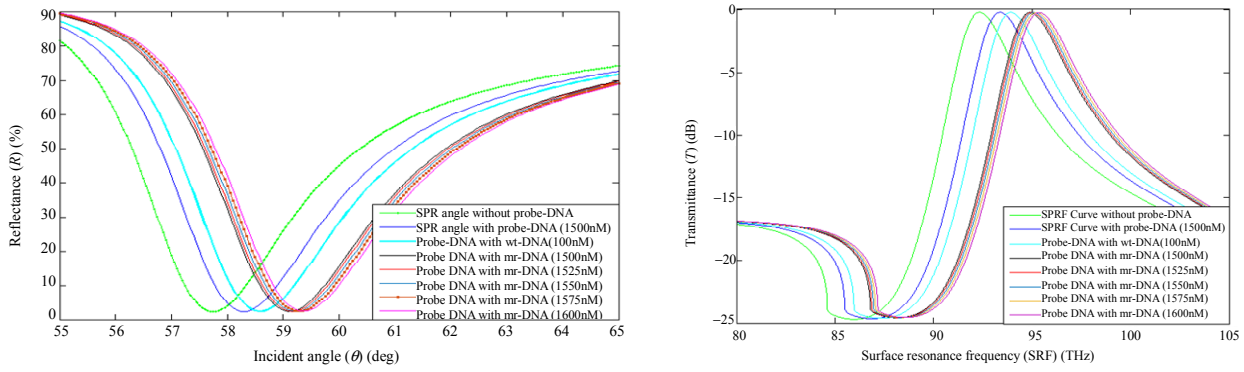

(a) (b)

Fig. 5 Change in characteristics curves for (a) SPR curve characteristics and (b) SPRF curve characteristics of the SPR sensor without pDNA, with pDNA and, with flowing different concentrated complementary target mrDNAs or mismatched target wtDNAs of BRCA1 and BRCA2 genes with PBS solutions.

Equation (15) is used to determine standard attributor's value, whose value is essential for proper detection of genetic biomarkers (916delTT and 6174delT) for early breast cancer recognized specific mutations of BRCA1 and BRCA2 genes.

$$\begin{aligned}
\delta R_{\min}^{\text{Cancer}} &= \left| R_{\min}^{\text{probe}} - R_{\min}^{\text{mr=1500}} \right| = 0.09 \\
\delta \theta_{\text{SPR}}^{\text{Cancer}} &= \left| \theta_{\text{SPR}}^{\text{probe}} - \theta_{\text{SPR}}^{\text{mr=1500}} \right| = 0.80 \text{ deg} \\
\delta T_{\max}^{\text{Cancer}} &= \left| T_{\max}^{\text{probe}} - T_{\max}^{\text{mr=1500}} \right| = 0.0083 \text{dB} \\
\delta SRF^{\text{Cancer}} &= \left| SRF^{\text{probe}} - SRF^{\text{mr=1500}} \right| = 1.52 \text{ THz}
\end{aligned} \quad . (15)$$

Equation (15) describes the minimum value of the breast cancer recognizing attributors, which are stetted equal to the right shift of SPR and SPRF curvatures after submersing mutated type target (1500 nm concentrated mrDNA sequence) DNA with probe DNA (shDNA). Concededly, Table 5 is the decision-making table, which can be applied for breast cancer detection, taking advantage of the detecting attributor's values. The minimum attributor values are $\delta R_{\min}^{\text{Cancer}}$ = 0.09, $\delta \theta_{\text{SPR}}^{\text{Cancer}}$ = 0.80 deg, $\delta T_{\max}^{\text{Cancer}}$ = 0.0083 dB, and $\delta SRF^{\text{Cancer}}$ = 1.52 THz for the detection of specific mutations in the PBS solution.

Table 5 Decision-making condition based upon different situations which happening to detecting attributors.

Decision-making condition (with respect to the change of $R_{\min}$, θ_{SPR}, $T_{\max}$, and SRF)			Decision
$\delta R_{\min}^{P-T} \geq \delta R_{\min}^{\text{Cancer}}$ & $\delta \theta_{\text{SPR}}^{P-T} \geq \delta \theta_{\text{SPR}}^{\text{Cancer}}$	or	$\delta T_{\max}^{P-T} \geq \delta T_{\max}^{\text{Cancer}}$ & $\delta SRF^{P-T} \geq \delta SRF^{\text{Cancer}}$	Cancer detected
$\delta R_{\min}^{P-T} < \delta R_{\min}^{\text{Cancer}}$ & $\delta \theta_{\text{SPR}}^{P-T} < \delta \theta_{\text{SPR}}^{\text{Cancer}}$		$\delta T_{\max}^{P-T} < \delta T_{\max}^{\text{Cancer}}$ & $\delta SRF^{P-T} < \delta SRF^{\text{Cancer}}$	No Cancer detected
$\delta R_{\min}^{P-T} \geq \delta R_{\min}^{\text{Cancer}}$ & $\delta \theta_{\text{SPR}}^{P-T} \leq \delta \theta_{\text{SPR}}^{\text{Cancer}}$		$\delta T_{\max}^{P-T} \leq \delta T_{\max}^{\text{Cancer}}$ & $\delta SRF^{P-T} \geq \delta SRF^{\text{Cancer}}$	Try again
$\delta R_{\min}^{P-T} \leq \delta R_{\min}^{\text{Cancer}}$ & $\delta \theta_{\text{SPR}}^{P-T} \geq \delta \theta_{\text{SPR}}^{\text{Cancer}}$		$\delta T_{\max}^{P-T} \geq \delta T_{\max}^{\text{Cancer}}$ & $\delta SRF^{P-T} \leq \delta SRF^{\text{Cancer}}$	Try again

When the changes of $\delta R_{\min}^{P-T}$, $\delta \theta_{\text{SPR}}^{\text{P-T}}$, $\delta T_{\max}^{P-T}$, and δSRF^{P-T} are greater than or equal to $\delta R_{\min}^{\text{Cancer}}$, $\delta \theta_{\text{SPR}}^{\text{Cancer}}$, $\delta T_{\max}^{\text{Cancer}}$, and $\delta SRF^{\text{Cancer}}$, specific mutations (916delTT and 6174delT) of BRCA1 and BRCA2 genes are sensed (breast cancer detected) by the SPR sensor, and if the changes of $\delta R_{\min}^{P-T}$, $\delta \theta_{\text{SPR}}^{\text{P-T}}$, $\delta T_{\max}^{P-T}$, and δSRF^{P-T} are smaller than $\delta R_{\min}^{\text{Cancer}}$, $\delta \theta_{\text{SPR}}^{\text{Cancer}}$, $\delta T_{\max}^{\text{Cancer}}$, and $\delta SRF^{\text{Cancer}}$, no breast cancer mutations are sensed; apart from both of these cases, no consistent consequence will be recognized, and the recognition technique should be resumed. A graphene implicated SPR sensor is used to make a decision from the achieved results, respectively in Table 5, which indicates the detection and can be utilized to confirm the detection of 916delTT and 6174delT mutations.

Finally, in this section, we analyze the electric field distribution by incorporating the FDTD technique by using commercial software Lumerical FDTD Solution. The FDTD is a powerful method to solve Maxwell's equations in a nano film layer (Au-50 nm) by using the YEE-algorithms. The FDTD method is more reliable than others, such as multiple-multiple or Green's dynamic method in solving Maxwell's equations for complex geometries and dispersive media, like gold and silver [33–36]. The simulation is carried out with the Gaussian-modulated continuous wave with the central wavelength of 633 nm. Surface plasmon polarition (SPP) excitation is performed by using the angular interrogation technique. The perfectly matched layer (PML) boundary condition is used in such a way that waves enter into the layers with generating the minimum reflections ($R_{\min}$). The reflected intensity is reported by using discrete Fourier transform (DFT) reflectance and transmission monitor at 200 nm away from the Au/graphene interface. We state the electric field distribution of the proposed biosensor structure with 10 graphene layers. In Fig. 6, it is observed that the normalized electric field can obtain greater absorption of light to have large SPW excitation,

and the numerical value of the electric field distribution in the configuration with graphene is greater. Therefore, SPW excitations are stronger for the configuration with graphene.

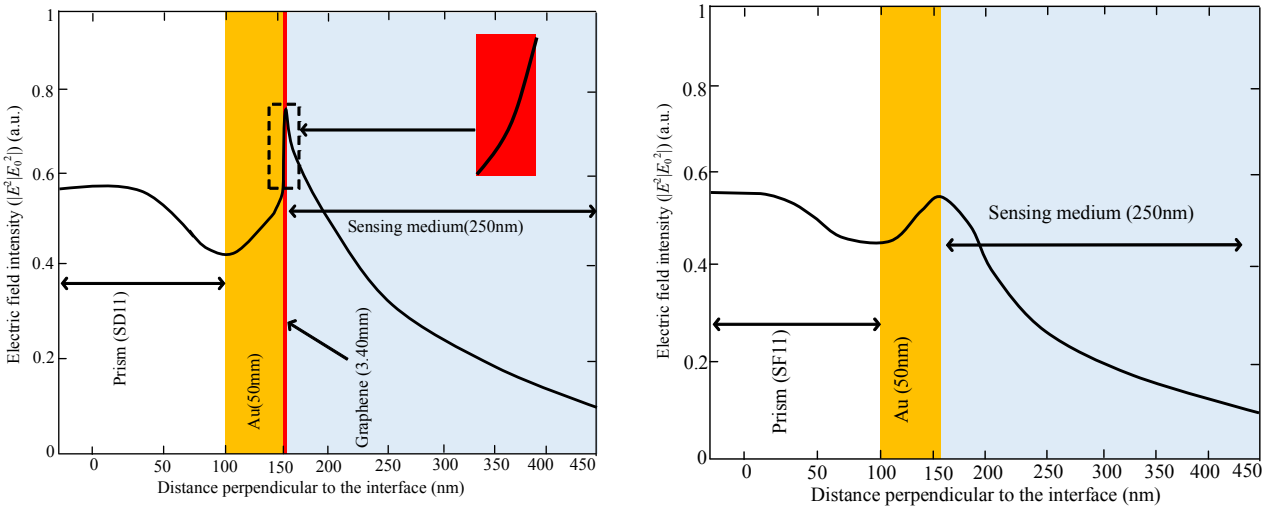

(a) (b)

Fig.6 Normalized electric field intensity (a) with (L=10) graphene layers and (b) without graphene layer.

The addition of 2D material (graphene) over the gold layer can affect the field intensity which causes the sensitivity enhancement by increasing the mobility of electrons [11–14]. The electric field intensity approaches to its maximum value when the reflectance curve shows the minimum value of reflectivity. In this case, the highest excitation of SPs can occur. As can be clearly seen from Fig. 6, the graphene layer increases the field intensity and displays a peak at the gold sensing medium interface which leads to the excitation of SPs at this interface.

4. Conclusions

We have presented a numerical modeling of the graphene-coated fiber optic SPR biosensor for proper detection of genetic biomarkers (916delTT and 6174delT) for early breast cancer detection by means of DNA hybridization. From the variations of the SPR angle and SPRF, the proposed sensor can differentiate perfectly matched and mismatched DNA interaction between the probe DNA and target DNA. Simulation results have shown that the use of graphene can be more effective compared with the usual SPR biosensors. This increased sensitivity is due to the absorption ability of graphene. This sensor has provided the easiest way of monitoring cancer tumor cell and confirming detection of specific mutations of BRCA1 and BRCA2 genes. Eventually, this sensor successfully distinguishes breast cancerous cell and non-cancerous cell. The thought offered in this article is expected to be understood easily, and because of the enhanced sensitivity, the proposed hybrid SPR biosensor has great prospective in future industrial applications of genetic biomarkers (916delTT and 6174delT) for early breast cancer detection. Finally, in this paper, we analyze the electric field distribution and observe that the graphene layer increases the field intensity and displays a peak at the gold sensing medium interface which leads to the excitation of SPs at this interface.

References

[1] D. A. Caporale and E. E. Swenson, "Two different BRCA2 mutations found in a multigenerational family with a history of breast, prostate, and lung cancers," *Advances in Genomics and Genetics*, 2014, 2014(4): 87–94.

[2] L. G. Carrascosa, A. Calle, and L. M. Lechuga, "Label-free detection of DNA mutations by SPR: application to the early detection of inherited breast cancer," *Analytical and Bioanalytical Chemistry*, 2009, 393(4): 1173–1182.

[3] M. B. Hossain, T. B. A. Akib, L. F. Abdulrazak, and M. M. Rana, "Numerical modeling of graphene-coated fiber optic surface plasmon resonance biosensor for BRCA1 and BRCA2 genetic breast cancer detection," *Optical Engineering*, 2019, 58(3): 037104.

[4] C. W. Lin and C. C. Chang, "Breast cancer detection using surface plasmon resonance-based biosensors," *Biosensors and Cancer*, 2012, chapter 12: 229–247.

[5] I. Godet and D. M. Gilkes, "BRCA1 and BRCA2 mutations and treatment strategies for breast cancer," *Integrative Cancer Science and Therapeutics*, 2017, 4(1): 1–17.

[6] Y. Li, A. W. Wark, H. J. Lee, and R. M. Corn, "Single-nucleotide polymorphism genotyping by nanoparticle-enhanced surface plasmon resonance imaging measurements of surface ligation reactions," *Analytical Chemistry*, 2006, 78(9): 3158–3164.

[7] M. B. Hossain and M. M. Rana, "Graphene coated high sensitive surface plasmon resonance biosensor for sensing DNA hybridization," *Sensor Letters,* 2016, 14(2): 145–152.

[8] A. K. Paul and A. K. Sarkar, "Dual-core photonic crystal fiber plasmonic refractive index sensor: a numerical analysis," *Photonic Sensors*, 2019, 9(2): 151–161.

[9] Y. Wang, S. Meng, Y. Liang, L. Li, and W. Peng, "Fiber-optic surface plasmon resonance sensor with multi-alternating metal layers for biological measurement," *Photonic Sensors*, 2013, 1(3): 202–207.

[10] A. K. Mishra, S. K. Mishra, and R. K. Verma, "Graphene and beyondgraphene MoS_2: a new window in surface-plasmon-resonance-based fiber optic sensing," *The Journal of Physical Chemistry C*, 2016, 120(5): 2893–2900.

[11] L. Wu, J. Guo, H. Xu, X. Dai, and Y. Xiang, "Ultrasensitive biosensors based on long-range surface plasmon polariton and dielectric waveguide modes," *Photonics Research*, 2016, 4(6): 262–266.

[12] L. M. Wu, J. Guo, X. Y. Dai, Y. J. Xiang, and D. Y. Fan, "Sensitivity enhancement by MoS_2-graphene hybrid structure in guided wave surface plasmon resonance biosensor," *Plasmonics*, 2018, 13(1): 281–285.

[13] L. M. Wu, J. Guo, Q. K. Wang, S. B. Lu, X. Y. Dai, Y. J. Xiang, *et.al.*, "Sensitivity enhancement by using few layer black phosphorus-graphene/TMDCs heterostructure structure in surface plasmon resonance biochemical sensor," *Sensors and Actuators B: Chemical*, 2017, 249(13): 542–548.

[14] L. M. Wu, Y. Jia, L. Y. Jiang, J. Guo, X. Y. Dai, Y. J. Xiang, *et.al.*, "Sensitivity improved SPR biosensor based on the MoS_2/graphene-aluminium hybrid structure," *IEEE Journal of Lightwave Technology*, 2017, 35(1): 82–87.

[15] B. X. Ruan, J. Guo, L. M. Wu, J. Q. Zhu, Q. You, X. Y. Dai, *et. al.*, "Ultrasensitive terahertz biosensors based on fano resonance of a graphene/waveguide hybrid structure," *Sensors*, 2017, 17(8): 19–24.

[16] P. Englebienne, A. Van Hoonacker, and M. Verhas, "Surface plasmon resonance: principles, methods and applications in biomedical sciences," *Journal of Spectroscopy*, 2003, 17(2–3): 255–273.

[17] M. Pumera, "Graphene in biosensing," *Materials Today*, 2011, 14(7–8): 308–315.

[18] M. B. Hossain, M. Hassan, L. F. Abdulrazak, M. M. Rana, M. M. Islam, and M. S. Rahman, "Graphene-MoS_2-Au-TiO_2-SiO_2 hybrid SPR biosensor for formalin detection: numerical analysis and development," *Advanced Materials Letters*, 2019: https://www.vbripress.com/aml/articles/details/1395.

[19] A. K. Geim and K. S. Novoselov, "The rise of graphene," *Nature Materias*, 2007, 6(3): 183–191.

[20] F. Bonaccorso, Z. Sun, T. Hasan, and A. C. Ferrari, "Graphene photonics and optoelectronics," *Nature Photonics*, 2010, 4(9): 611–622.

[21] L. Wu, Y. Jia, L. Jiang, J. Guo, X. Dai, and Y. Xiang, *et. al.*, "Sensitivity improved SPR biosensor based on the MoS_2/graphene-aluminum hybrid structure," *Journal of Lightwave Technology*, 2017, 35(1): 82–87.

[22] M. B. Hossain and M. M. Rana, "DNA hybridization detection based on resonance frequency readout in graphene on Au SPR biosensor," *Journal of Sensors,* 2016, 16: 6070742.

[23] V. Ball and J. J. Ramsden, "Buffer dependence of refractive index increments of protein solutions," *Biopolymers*, 1998, 46(7): 489–492.

[24] L. Diéguez, N. Darwish, M. Mir, E. Martínez, M. Moreno, and J. Samitier, "Effect of the refractive index of buffer solutions in evanescent optical biosensors," *Sensor Letters*, 2009, 7(5): 851–855.

[25] K. N. Shushama, M. M. Rana, R. Inum, and M. B. Hossain, "Graphene coated fiber optic surface plasmon resonance biosensor for the DNA hybridization detection: Simulation analysis," *Optics Communications*, 2017, 383: 186–190.

[26] J. Homola and M. Piliarik, "Surface plasmon resonance (SPR) sensors: approaching their limits," *Optics Express*, 2009, 17(19): 16505–16517.

[27] J. S. del Río, L. G. Carrascosa, F. J. Blanco, M.

Moreno, J. Berganzo, A. Calle, *et al.*, "Lab-on-a-chip platforms based on highly sensitive nanophotonic Si biosensors for single nucleotide DNA testing," *Silicon Photonics II*, 2007, 6477: 64771B.

[28] M. B. Hossain, M.M. Rana, L. F. Abdulrazak, S. Mitra, and M. Rahman, "Graphene-MoS_2 with TiO_2-SiO_2 layers based surface plasmon resonance biosensor: numerical development for formalin detection," *Biochemistry and Biophysics Reports,* 2019, 18: 100639.

[29] M. S. Rahman, M. S. Anower, M. R. Hasan, M. B. Hossain, and M. I. Haque, "Design and numerical analysis of highly sensitive Au-MoS_2-graphene based hybrid surface plasmon resonance biosensor," *Optics Communications*, 2017, 396: 36–43.

[30] M. S. Rahman, M. S. Anower, M. K. Rahman, M. R. Hasan, M. B. Hossain, and M. I. Haque, "Modeling of highly sensitive MoS_2-graphene hybrid based fiber optic SPR biosensor for sensing DNA hybridization," *Optik*, 2017, 140: 989–997.

[31] L. Wu, H. S. Chu, W. S. Koh, and E. P. Li, "Highly sensitive graphene biosensors based on surface plasmon resonance," *Optics Express*, 2010, 18(14): 14395–14400.

[32] A. Chakraborty, D. Banerjee, J. Basak, and A. Mukhopadhyay, "Absence of 185delAG and 6174delT mutations among breast cancer patients of eastern India," *Asian Pacific Journal of Cancer Prevention*, 2015, 16(17): 7929–7933.

[33] M. B. Hossain, S. Muktadhir, and M. M. Rana, "Multi-structural optical devices modeling using graphene tri-layer sheets," *Optik*, 2016, 127(15): 5841–5851.

[34] M. B. Hossain, M. S. Muktadhir, and M. M. Rana, "Modeling graphene macroscopic and microscopic conductivity in the sub-cell FDTD method," In *International Conference on Electrical & Electronic Engineering (ICEEE)*, Rajshahi, Bangladesh, 2015, 15838474.

[35] M. M. Rana, M. B. Hossain, M. R. Islam, and Y. G. Guo, "Surface plasmon polariton propagation modeling for graphene parallel pair sheets using FDTD," in *2015 IEEE International Conference on Applied Superconductivity and Electromagnetic Devices (ASEMD)*, Shanghai, China, 2015, 15953521.

[36] M. B. Hossain and M. M. Rana, "An effective compact-FDTD wideband modeling of graphene conductivity," in *2015 International Conference on Electrical Engineering and Information Communication Technology (ICEEICT)*, 2015, Dhaka, Bangladesh, 15570584.